energy&fuels

ARTICLE

pubs.acs.org/EF

Investigation of Chemical Looping Combustion of Coal with $CuFe_2O_4$ Oxygen Carrier

Baowen Wang,*[,†,‡] Rong Yan,[§] Haibo Zhao,[†] Ying Zheng,[†] Zhaohui Liu,[†] and Chuguang Zheng[†]

[†]State Key Laboratory of Coal Combustion, Huazhong University of Science and Technology, Wuhan 430074, People's Republic of China

[‡]College of Electric Power, North China University of Water Conservancy and Hydroelectric Power, Zhengzhou 450011, People's Republic of China

[§]Institute of Environmental Science and Engineering, Nanyang Technological University, Innovation Center, Block 2, Unit 237, 18 Nanyang Drive, Singapore 637723, Singapore

ABSTRACT: Chemical looping combustion (CLC) has great advantages to obtain pure CO_2 from coal combustion flue gas at a manageable cost. $CuFe_2O_4$ was put forward as a novel oxygen carrier, which integrated Cu and Fe metals into one oxide matrix with superior characteristics over single metal oxide of either CuO or Fe_2O_3 and had a high potential to be used in CLC. In this study, the reaction of $CuFe_2O_4$ with two Chinese coals of different ranks [Liu Pan Shui (LPS) sub-bituminous coal and Yang Quang (YQ) anthracite] was performed in a thermogravimetric analyzer (TGA). Fourier transform infrared (FTIR) spectroscopy was used to detect *in situ* the emitted gases from the TGA. Field scanning electron microscopy/energy-dispersive X-ray spectrometry (FSEM/EDX) was used to study the morphology and elemental compositions present in the solid residues, and the related phases were further identified by X-ray diffraction (XRD). Meanwhile, to explore the reaction mechanisms involved for the reaction of $CuFe_2O_4$ with coal, a more realistic simulation system with 376 species was designed for thermodynamic analysis. Through all of these measures, it was found that the reaction of LPS lean coal with $CuFe_2O_4$ underwent two distinct reaction stages at 300−600 and 600−850 °C, respectively. At these two reaction stages, $CuFe_2O_4$ was dominantly reduced into Cu and Fe_3O_4 by transfer of the lattice oxygen [O] in $CuFe_2O_4$, and then the formed Fe_3O_4 was further reduced into $Fe_{2.962}O_4$. However, above 800 °C, $CuFeO_2$ and Cu_2O were produced through direct decomposition of $CuFe_2O_4$ into $CuFeO_2$ and then further partial decomposition of $CuFeO_2$ into Cu_2O. Especially, O_2 generated was greatly beneficial to the full conversion of the remaining coal. Different from LPS, the reaction of YQ with $CuFe_2O_4$ presented only one discernible reaction stage above 600 °C. Besides Cu and $CuFeO_2$, $Fe_{2.957}O_4$ was also generated. Furthermore, four cycles of reduction of $CuFe_2O_4$ with H_2 and then oxidation with air displayed a good reaction stability of synthesized $CuFe_2O_4$. However, if coal was used, iron silicates were formed from the interaction of the reduced $CuFe_2O_4$ with ash and resulted in the insufficient reoxidation of reduced $CuFe_2O_4$. As such, effective separation of coal ash should be included in the CLC process to ensure the full regeneration of reduced $CuFe_2O_4$.

1. INTRODUCTION

Anthropogenic CO_2 emission from fossil fuel combustion, especially coal, has been considered as one of the main contributors to the rapid increase of the atmospheric CO_2 concentration. Effective measures to capture CO_2 from fossil fuel combustion should thus be immediately taken in response to the ever-increasing detrimental consequences of the greenhouse effect and global warming. In comparison to all of the other existing techniques, chemical looping combustion (CLC) has instigated great interest for its verified advantages, such as the inherent separation of CO_2 without any extra energy consumption and thorough eradication of the formation of thermal NO_x.[1] In CLC, coal is first introduced into a fuel reactor (FR) and fully oxidized with an oxygen carrier (OC) instead of air, and then at its full conversion, pure CO_2 will be available for sequestration after condensation of the exit gas from the FR; thus, any extra gas separation process is avoided. Finally, the reduced OC is transported back to an air reactor (AR) and oxidized by air for the following cycle of reaction with coal in the FR.

Currently, several investigations on the lab-scaled fluidized facility from different institutions have demonstrated the feasibility of direct use of coal as fuel for CLC application. It was found that the main rate-limiting step involved was actually the gasification of coal, especially the coal residue left after gasification, instead of the reduction of OC with the coal gasification products generated *in situ*. Meanwhile, Fe_2O_3 as an OC was also found active enough to react with coal in the real coal-based CLC system.[2−4] In view of maintaining a sufficient FR temperature for a high gasification rate, CuO as an OC has been valued for its exothermic characteristics in the reduction reaction with coal and extensively studied.[5−8] Nevertheless, various limitations of CuO discouraged its application as an OC in CLC, such as the low melting point of the reduced counterpart Cu, its high cost, and its harmful impact to both health and the environment.[9] Therefore, a new oxygen carrier, $CuFe_2O_4$, was first proposed, which has the exothermic characteristics of CuO as well as the lower cost and lower toxicity of Fe_2O_3, and thus, it would be of great significance to CLC of coal.

Received: March 15, 2011
Revised: June 10, 2011
Published: June 15, 2011

Table 1. Proximate and Ultimate Analyses of Coal Samples

samples	proximate analysis[a] (wt %)				ultimate analysis (wt %, db[b])					LHV[d] (MJ/kg)
	M_{ad}	V_{ad}	A_{db}	FC_{ad}	C	H	N	S	O[c]	
LPS	3.09	22.84	25.38	48.69	62.89	2.31	1.27	0.89	32.64	23.49
YQ	2.39	8.05	29.24	60.32	64.02	1.81	1.1	0.67	32.40	22.71

[a] *M*, moisture content; *V*, volatile matter; *A*, ash content; FC, fixed carbon; ad, air-dried basis. [b] Dry basis. [c] The O content was determined by difference. [d] Lower heating value.

Table 2. Ash Analysis of Coal Samples (wt %)

samples	SiO_2	Al_2O_3	Fe_2O_3	SO_3	CaO	TiO_2	Co_3O_4	K_2O	MgO	Na_2O
LPS	41.31	24.07	17.0	4.60	3.12	2.80	2.02	1.41	1.58	0.63
YQ	68.49	14.58	4.48	4.10	3.65	0.69	0.52	1.04	0.63	1.24

For the CLC of coal, it is critical to improve the gasification of coal and ensure its full conversion. Previous studies have addressed this issue at different levels. Using a thermogravimetric analyzer (TGA), Siriwardane et al.,[8] Cao et al.,[10] and Zhao et al.[11] studied the reaction of different coals or chars with various metal oxides. However, because of the complexity of the reaction involved, the reduction mechanisms of the OC with coal are still not completely understood and it is worthwhile to further explore them to maximize the use of coal in the realistic CLC system.

In addition, after the full reaction of coal with metal OC, the effective separation of the reduced OC from coal ash should be addressed. The interaction between the reduced OC and ash components has been shown to form some inert compounds and, thus, deteriorated its reactivity.[2,8,11−13] Meanwhile, the melting point of the resulting ash was lowered, and agglomeration of the reduced OC with ash possibly arose, which made it difficult to separate the reduced OC from the resulting coal ash. Therefore, it is also important to understand the ash effect on the reactivity of OC and the possible interactions involved.

In this study, the reduction of $CuFe_2O_4$ OC with two Chinese coals of different ranks was investigated using TGA. The emitted gases were evaluated using Fourier transform infrared (FTIR) spectroscopy coupled with TGA. Thermodynamic simulation of the reduction of $CuFe_2O_4$ with coal was further conducted to explore the reaction mechanism involved. Finally, the morphology and chemical properties of the reduced OC products were characterized using Field scanning electron microscopy/energy-dispersive X-ray spectrometry (FSEM/EDX), and their phases were further identified by X-ray diffraction (XRD). Overall, this study could provide useful information for establishing a practical coal-based CLC system through a better understanding of the mechanisms involved.

2. EXPERIMENTAL SECTION

2.1. Materials and Characterization. Two Chinese coals of different ranks were selected, including Liu Pan Shui sub-bituminous coal and Yang Quang anthracite, hereafter abbreviated as LPS and YQ, respectively. The original samples were first dried at 105 °C overnight, then ground, and sieved to collect the samples in 63−106 μm size range for the ensuing use. The proximate and ultimate analyses of the two prepared coal samples are presented in Table 1. It was found that, with the enhanced rank of LPS coal as compared to YQ coal, the content of volatile matter and the ratio of H/C decreased, while the content of fixed carbon increased. The ash contents of the two coals increased from 25.38% in LPS to 29.24% in YQ, but contrarily, the lower heating value (LHV) decreased from 23.49 to 22.7 MJ/kg. Furthermore, the ash components of the two coal samples used were tested using X-ray fluorescence (XRF, Philips, PW 2400, Almelo, The Netherlands), and the results are provided in Table 2. Minerals containing Si, Al, and Fe elements were found to be the three major components, and their total content was more than 80 wt % for both coal ashes.

Besides coal samples, three pure oxides, including $CuFe_2O_4$, CuO, and Fe_2O_3 used in this research, were synthesized by the novel sol−gel combustion synthesis (SGCS) method. The hydrated metal nitrates and urea were used as the precursors. The procedure of SGCS was briefly described below. First, the stoichiometric compositions of metal nitrates (including nitrates of iron and copper) and urea were calculated, and then the accurately weighted nitrates and urea were dissolved in deionized (DI) water sequentially. The mixture was then stirred on a hot plate in air and aged at 75 °C until a viscous colloid was formed. After that, the wet sol was dried at ∼135 °C in a desiccator overnight, then transferred to a ceramic dish, and ignited in a preheated muffle furnace at 600 °C for 15 min. Finally, the as-ignited product proceeded to be sintered in the same furnace at 950 °C for 2 h. The detailed procedure of SGCS and the characterization of the formed oxides were elaborated elsewhere.[14] Similarly, after grinding and sieving, the oxides in the range of 63−106 μm were used. Finally, the as-prepared oxides were evenly mixed with coal at the designed mass ratio (as seen below in section 2.2) in a laboratory mortar.

2.2. Determination of the Oxygen Excess Number Φ for Different Coal Samples. The full conversion of coal is dependent upon the availability of oxygen present in the OC. A sufficient supply of the OC is very important to operate the CLC system. The method of coal mass balance[10] was adopted to determine the amount of $CuFe_2O_4$ OC to be introduced into the CLC system. According to the results of proximate and ultimate analyses of coal, the weight fractions of hydrogen and oxygen in the moisture were deducted. If 1 kg of coal sample was used, the content of different atoms (including C, H, O, N, and S) contained in the coal samples could be determined and the relative chemical formula was represented as $C_\alpha H_\beta S_\gamma O_\delta (N_2)_\nu$. For $CuFe_2O_4$, supposing the reduced counterpart was Cu and Fe_3O_4 when the coal was fully converted, the reduced reaction of $CuFe_2O_4$ with different coal samples could be depicted as in eq 1.

$$\begin{aligned} &C_\alpha H_\beta S_\gamma O_\delta (N_2)_\nu + 3(\alpha+\beta/4+\gamma-\delta/2)/2CuFe_2O_4 \\ &\rightarrow 3(\alpha+\beta/4+\gamma-\delta/2)/2Cu + (\alpha+\beta/4+\gamma-\delta/2)Fe_3O_4 \\ &+ \alpha CO_2(g) + \beta/2H_2O(g) + \gamma SO_2(g) + \nu N_2(g) \end{aligned} \quad (1)$$

From eq 1, the theoretical stoichiometric oxygen needed for the full conversion of coal is determined as $3(\alpha+\beta/4+\gamma-\delta/2)/2$. Supposing the realistic oxygen contained in the OC was $Y(O)$, then the oxygen excess number Φ was defined as follows:

$$\Phi = Y(O)/(3(\alpha+\beta/4+\gamma-\delta/2)/2) \quad (2)$$

In eq 2, a value of Φ = 1 meant that the $CuFe_2O_4$ OC supplied just met the requirement of the full conversion of coal. According to the aforementioned method, the relative chemical formulas of LPS and YQ

of 1 kg could be depicted as $C_{37.9}H_{14.1}N_{0.66}S_{0.2}O_{13.5}$ and $C_{36.8}H_{10.2}N_{0.54}S_{0.144}O_{13.1}$, respectively. Then, on the basis of eq 2, if $\Phi = 1$, the mass ratios of $CuFe_2O_4$ to LPS and YQ were corresponding to 24.1 and 22.8, respectively.

2.3. Experimental Methods. The reaction characteristics of the synthesized $CuFe_2O_4$ OC with two different coals at the oxygen excess number $\Phi = 1$ were investigated using TGA (TA 2050, TA Instruments, New Castle, DE). The mixture of coal and $CuFe_2O_4$ OC was heated from ambient to 150 °C at 10 °C/min and held at this temperature for up to 10 min to fully remove the moisture. Then, it was further heated to 850 °C at 35 °C/min with holding at this temperature for 10 min to ensure the sufficient conversion of coal. A N_2 atmosphere was provided, and the flow rate of N_2 and the total mass for the mixture of coal and OC were determined at 50 mL/min and ~15 mg after several pre-screening experiments to eliminate the potential impact of mass transfer between gas and solid phases.

The evolved gases from the reaction of coal with $CuFe_2O_4$ OC in the TGA were first dried through a portable tubular gas desiccator full of $Ca(SO_4)\cdot 2H_2O$, and then detected *in situ* by a FTIR spectrometer equipped with a deuterated triglycine sulfate (DTGS) detector (BioRad Excalibur Series, model FTS 3000). The scanning range of IR was 4000−500 cm^{-1}, and the resolution and sensitivity were preset at 4 cm^{-1} and 1, respectively.

Furthermore, to examine the reaction stability of $CuFe_2O_4$ over multicycles of reduction and oxidation, H_2 was selected as fuel first, and four cycles of the reduction of $CuFe_2O_4$ with 50 vol % H_2 and then oxidation with air were conducted in the TGA (TA 2050, TA Instruments, New Castle, DE). The total gas flow rate was fixed at 50 mL/min. The detailed experimental procedures were described below. First, 15 mg of $CuFe_2O_4$ was heated in N_2 at 35 °C/min until the final temperature of 850 °C was reached. Then, the N_2 flow was switched to H_2 flow, and the reduction of $CuFe_2O_4$ with H_2 was initiated and sustained for 8 min. Hereafter, N_2 flow was introduced back again to sweep the remaining H_2 away for 2 min to avoid the potential explosion of H_2 mixed with air to be used later. Finally, air was introduced to start the oxidation of the reduced $CuFe_2O_4$ with air for 3 min. The same processes were repeated 4 times.

Meanwhile, to further investigate the reaction performance of $CuFe_2O_4$ with coal over many cycles of the redox process, LPS coal was selected as the model fuel and reduction of $CuFe_2O_4$ with LPS for an extended duration of 30 min and then oxidation with air for 10 min were conducted in the same TGA setup at the heating rate of 35 °C/min. N_2 was used as the carrier gas throughout the whole reduction stage of $CuFe_2O_4$ with LPS, and the final temperature was elevated to 900 °C other than 850 °C to ensure the full conversion of coal. However, it was different from the reaction of $CuFe_2O_4$ with H_2. Redox experiments of $CuFe_2O_4$ with LPS and then with air were quite difficult, because after each redox reaction, the same amount of coal consumed in the previous redox experiment should be accurately weighed and evenly mixed with the reduced counterpart of $CuFe_2O_4$. Therefore, only two cycles of the redox reaction for the reduction of $CuFe_2O_4$ with LPS and then oxidation with air were conducted, which is similar to the methodology adopted above for the redox reactions of $CuFe_2O_4$ with H_2 and air.

Finally, the morphology and elemental composition of the solid products from the reaction of coal with $CuFe_2O_4$ were studied using FSEM (Siron 200, Roosendaal, The Netherlands) coupled with an EDX (Genesis, EDAX, Inc., Mahwah, NJ) at a magnification of 800× and an accumulated voltage of 30 kV. The formed phases were further identified by XRD (X'Pert PRO, Almelo, The Netherlands) with 40 kV and 40 mA Cu Kα (λ = 0.154 Å) radiation and at the step-scanned range of 10−80°.

2.4. Conversion of $CuFe_2O_4$ OC with Coal. The reaction of $CuFe_2O_4$ OC with coal was very complicated and consisted of coal pyrolysis and gasification as well as the reactions of $CuFe_2O_4$ with gaseous products from coal and the remaining char. To illuminate the role of $CuFe_2O_4$ in its reaction with coal, several conversion indexes were defined below.

First, $CuFe_2O_4$ was reacted with gasification products of coal into CO_2 and H_2O, and the produced CO_2 and H_2O in turn acted as good gasifying agents and promoted the gasification of coal as well as more gasification products of coal to react with $CuFe_2O_4$ OC. Thus, to reflect the interaction of coal with the OC, the mixture conversion index of coal with OC, $X_{coal-OC}$, was defined in eq 3[15,16]

$$X_{coal-OC}(t) = \frac{W_{coal-OC}(t = 0) - W_{coal-OC}(t)}{x_1 \Delta W_{OC} + x_2 \Delta W_{coal}} \quad (3)$$

$$f = x_1/x_2 \quad (4)$$

where $X_{coal-OC}$ is the mixture conversion index for coal with OC (%), in which LPS and YQ are involved for coal, while three oxides, such as $CuFe_2O_4$, CuO, and Fe_2O_3, are included for OC, $W_{coal-OC}(t = 0)$ and $W_{coal-OC}(t)$ are the initial and instantaneous weight losses for the mixture of coal with the OC used (wt %), x_1 and x_2 are the mass fractions of OC and coal in their mixture (wt %), f is the mass ratio of the OC/coal, and ΔW_{OC} and ΔW_{coal} denote the maximal weight losses of the OC and coal, respectively.

Furthermore, to reveal the real limiting step for the reaction of coal with the OC based on the reference cases of coal pyrolysis under N_2 and coal combustion under air, the conversion index of the OC alone present in its mixture with coal, X_{OC}, is defined. According to the conservation of the total weight throughout the whole reaction process for the OC with coal, the OC conversion index X_{OC} could be expressed in eqs 5 and 6 as follows:

$$W_{coal-OC}(t) = x_1 W_{OC}(t) + x_2 W_{coal}(t) \quad (5)$$

$$X_{OC} = \frac{W_{coal-OC}(t) - x_2 W_{coal}(t)}{x_1 \Delta W_{OC}} \quad (6)$$

where $W_{OC}(t)$, $W_{coal}(t)$, and $W_{coal-OC}(t)$ are the instantaneous weight losses for the coal, OC, and their mixture at the time t. The meanings of the other characters in eqs 5 and 6 are the same as those in eqs 3 and 4.

2.5. Thermodynamic Simulation of the Reaction of $CuFe_2O_4$ with Coal. Although thermodynamic equilibrium analysis has great limitations and does not consider kinetic constraints in the real process, such as turbulent mixing and temperature gradients,[17] the equilibrium calculation would be a great help to better understand the lattice oxygen transfer and coal evolution. Thus, on the basis of the minimization of the total Gibbs free energy, the reaction of $CuFe_2O_4$ with coal was further simulated using the HSC Chemistry software, version 4.1. According to the characteristics for two Chinese coals LPS and YQ, including their proximate and ultimate analyses in Table 1 as well as ash analysis in Table 2, a complex reaction system with 376 species in total was established, as shown in Table 3. Noteworthy is that, in this equilibrium simulation, the coal was considered to consist of the main matrix elements (such as C, H, N, S, and O) as well as various minerals. Seven categories of compounds involved for the minerals present in coal were subdivided, such as oxides and various species of hydroxyl-, carbon-, sulfur-, silicon-, aluminum-, and titanium-based compounds. This simulation with seven categories of mineral compounds included was more realistic than other equilibrium simulations, where Siriwardane et al.[8] simulated the interaction between the model fly ash (only SiO_2 and Al_2O_3 considered) with different OCs, while Saha and Bhattacharya[18] simulated the reaction of a Victorian brown coal with NiO without considering the effect from the minerals present in that coal.

3. RESULTS AND DISCUSSION

3.1. Baseline Experiment by Coal without OC. To better understand the reaction of coal with $CuFe_2O_4$, the baseline tests

Table 3. Species Considered in the HSC Calculation for the Reaction of $CuFe_2O_4$ with Coal

coal		C	H	O	N	S
minerals	oxides	Fe_2O_3, Fe_3O_4, FeO; Cu_2O, CuO; $CuFeO_2$; SiO_2; Al_2O_3; CaO, CaO_2; MgO, MgO_2; K_2O, Co_3O_4, CoO; NaO, Na_2O_2; TiO_2, Ti_2O_3, Ti_3O_5, Ti_4O_7, etc.				
	hydroxy-based species	$Fe(OH)_2$, $Fe(OH)_3$; $Cu(OH)_2$; $Al(OH)_3$; $Ca(OH)_2$; $Co(OH)_2$; KOH; $Mg(OH)_2$; NaOH, etc.				
	carbon species	Fe_3C, $Fe_3C(A)$, $FeCO_3$; $CuCO_3$; CaC, $CaCO_3$, CaC_2O_4; K_2CO_3; $MgCO_3$, $MgCO_3*_3H_2O$; Na_2CO_3, $NaHCO_3$, $Na_2C_2O_4$, $Na_2CO_3*_3NaHCO_3$, $Na_2CO_3*NaHCO_3*_2H_2O$; $FeCO_3$, etc.				
	sulfur species	CuS, Cu_2S, $CuSO_4$, Cu_2SO_4; $Fe_2(SO_4)_3$, $FeSO_4$, FeS, FeS_2, $CuFeS_2$, CaS, $CaSO_3$, $CaSO_4$; CuS, Cu_2S, $CuSO_4$, Cu_2SO_4; K_2SO_4, etc.				
	silicon species	FeSi, $FeSi_2$, Fe_3Si, Fe_5Si_3, $FeSiO_3$, Fe_2SiO_4, CaSi, $CaSi_2$, Ca_2Si, $CaSiO_3$, Ca_3SiO_5, Ca_3SiO_7, $CaSiO_4$, etc.				
	aluminum species	$CuAl_2O_4$, $CuAlO_2$; $FeAl_2O_4$; $CaAl_2$, $CaAl_4$, $Ca_2Al_2O_5$, $CaO*2Al_2O_3$, $2CaO*2Al_2O_3$, etc.				
	titanium species	FeTi, Fe_2Ti, Fe_2TiO_4, Fe_2TiO_5; $Ca_3Ti_2O_7$, $CaO*TiO_2$, $CaO*3TiO_2$, etc.				
oxygen carrier		$CuFe_2O_4$				
gaseous species		CH_4, C_2H_4, C_2H_6, CO, CO_2, COS, CN, CN_2, CS_2; H_2, H_2O, HCN, H_2S; O, O_2; NO, NO_2, N_2O_4, N_2O_5; S_1-S_8, SO, SO_2, SO_3, etc.				

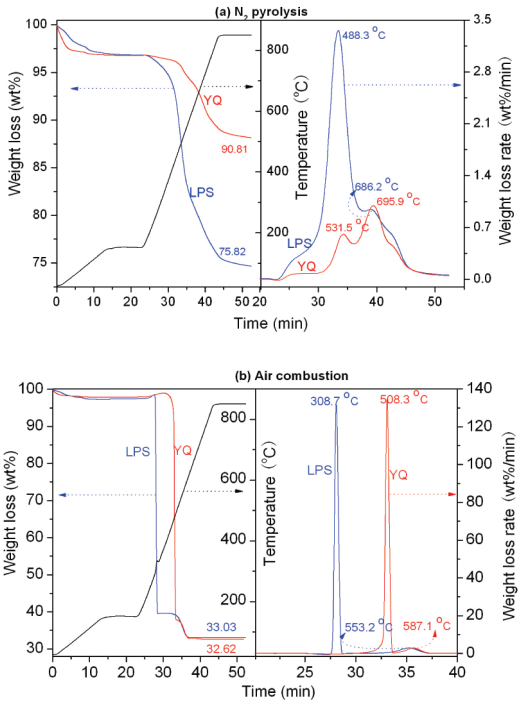

Figure 1. Reaction of two Chinese coals (LPS and YQ) under different atmospheres: (a) N_2 and (b) air.

of two Chinese coals of different ranks (LPS and YQ) under N_2 or air atmosphere were first performed in the TGA at the heating rate of 35 °C/min for reference, with focus on the effect of the coal rank. The results of mass loss [i.e., thermogravimetry (TG) curve] and the corresponding differential mass loss rate [i.e., differential thermogravimetry (DTG) curve] are plotted in panels a and b of Figure 1, respectively.

From Figure 1a, the pyrolysis of LPS was observed to occur around 200−800 °C. After the dehydration below 200 °C, LPS mainly underwent two different pyrolysis stages. The primary pyrolysis fell into 200−630 °C, with the characteristic temperature T_m (i.e., the peak temperature relative to the DTG maximum) residing at 488 °C. Approximately 20% volatile matter was emitted, which was possibly related to the breakage and reuniting of the organic functional groups.[19] The emitted gaseous species were identified as CH_4, C_2H_6, CO_2, H_2O, etc. by FTIR analysis in Figure 3a. After that, with the temperature elevated further from 630 to 850 °C, another small weight loss occurred at ∼686 °C with less than 5 wt % volatile matter emitted, because of the cleavage of the main carbon matrix.[19]

Different from LPS, the pyrolysis of YQ underwent two distinct stages, and the corresponding two characteristic temperatures T_m were increased to 531.5 and 695.9 °C. YQ pyrolysis at the latter stage was responsible for more weight loss than the former stage, which was due to the enhanced coal rank from LPS to YQ and the great decrease of the volatile content from 22.84 to 8.05 wt % (as shown in Table 1).[20]

Furthermore, from Figure 1b, for the combustion of LPS and YQ under air at 35 °C/min, either LPS or YQ burned quickly and emitted a large amount of CO_2, as evidenced in Figure 3b. The final residual weights left were 33.03 and 32.62 wt %. Both coals presented two-staged combustion, with the first distinct DTG peak approaching 140 wt %/min; however, the second stage was nearly indiscernible, and its DTG peak was as low as 2.8 wt %/min. In addition, the two characteristic temperatures of YQ combustion were 508.3 and 587.1 °C, far bigger than those of LPS, further indicating that the reactivity of YQ was lower than that of LPS.

3.2. Investigation of the Reaction of $CuFe_2O_4$ OC with Two Chinese Coals. *3.2.1. TGA−FTIR Analysis of the Reduction Reaction of $CuFe_2O_4$ with Coal.* The reactions of two coals with $CuFe_2O_4$ at the oxygen excess number $\Phi = 1$ under N_2 atmosphere were performed in the TGA at the same heating rate of 35 °C/min. The results of TG and DTG analyses are shown in panels a and b of Figure 2, respectively. Meanwhile, for comparison, results for the reactions of these two Chinese coals with Fe_2O_3 and CuO are also provided in panels c and d of Figure 2, respectively.

From Figure 2a, at 280−850 °C, LPS reacted with $CuFe_2O_4$ earlier and achieved a higher weight loss (up to 5 wt %) than YQ. In Figure 2b, two reaction stages at the peak temperatures of 471 and 825 °C were observed for the reaction of LPS with $CuFe_2O_4$. Especially, the mass loss rate at the latter stage was 0.5327 wt %/min, much higher than that of the former. Furthermore, judging from

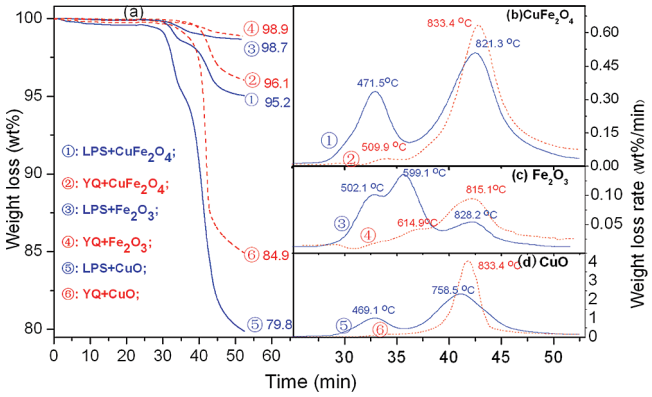

Figure 2. Reaction of two Chinese coals (LPS and YQ) with different OCs: (a) weight loss, (b) weight loss rate of $CuFe_2O_4$ with coal, (c) weight loss rate of Fe_2O_3 with coal, and (d) weight loss rate of CuO with coal.

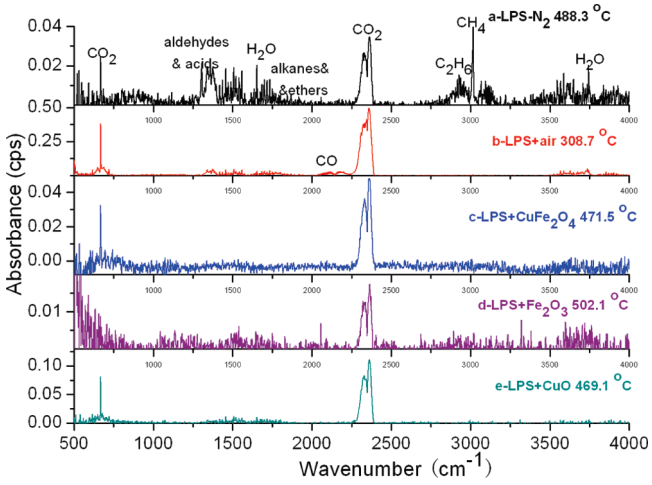

Figure 3. FTIR spectra of gas products from the reaction of LPS with different OCs, including $CuFe_2O_4$, CuO, and Fe_2O_3.

the FTIR analysis shown in Figure 3c, the first stage at 471 °C was attributed to the reaction of $CuFe_2O_4$ with LPS by emitting mainly CO_2 and water. Meanwhile, a two-dimensional (2D) IR plot of the gaseous products with CO_2 for the reaction of LPS with $CuFe_2O_4$ in Figure 4c further confirmed this observation, where CO_2 resided at the wavenumber around 2380 cm^{-1} and steam resided at the wavenumbers around both 1600 and 3600 cm^{-1}.

However, different from LPS, the reaction of YQ with $CuFe_2O_4$ displayed a single identifiable reaction stage, and the maximum mass loss rate was 0.6950 wt %/min at the peak temperature of 830 °C. Relative to Fe_2O_3 OC, the reactivity of LPS or YQ with $CuFe_2O_4$ OC was improved, and more CO_2 would thus be spontaneously generated, which was beneficial to the coal gasification and its further reaction with the $CuFe_2O_4$ OC. Furthermore, the increased reactivity would mean a shorter residence time of coal in the FR and, thus, a decrease of the required height of the FR in the CLC system.

3.2.2. Conversions of $CuFe_2O_4$ OC. To reveal the interaction between coal and OC based on the TG experimental results for coal pyrolysis and combustion without OC in Figure 1 and for the reaction of coal with different OCs (including CuO, Fe_2O_3, and $CuFe_2O_4$) in Figure 2, two conversion indexes, such as OC conversion alone in its mixture with coal as X_{OC} and the mixture conversion for the total mixture of coal with OC $X_{coal-OC}$, were calculated using eqs 3 and 6, respectively. The calculated results are presented in Figure 5.

First, from Figure 5a, the initiation reaction time of LPS with $CuFe_2O_4$ was around 30 min, far earlier than that of YQ with $CuFe_2O_4$ at ~40 min. Meanwhile, such a trend could also be observed for the reaction of LPS with either Fe_2O_3 in Figure 5b or CuO in Figure 5c, and their initiation reaction times also occurred around 30 min, 5 min earlier than that of YQ. This fact implied that the initiation of coal to react with different OCs was mainly determined by the reactivity of coal in the real CLC system.[3,21−24] Thus, low-rank coal with good reactivity should be preferred.

Furthermore, among all of the mixture conversions $X_{OC + coal}$ for different OCs (including $CuFe_2O_4$, CuO, and Fe_2O_3) with two Chinese coals, LPS or YQ, in Figure 5, the mixture conversion index of Fe_2O_3 with YQ was the lowest. Meanwhile, as shown in Figure 5b, although the mixture conversion index of Fe_2O_3 with LPS $X_{LPS + Fe_2O_3}$ was bigger than that of YQ with Fe_2O_3 $X_{YQ+ Fe_2O_3}$, $X_{LPS + Fe_2O_3}$ only reached 3.06% and was much less than the mixture conversion index of LPS with CuO $X_{LPS + CuO}$, which reached as high as 71.07%. Obviously, the reactivity of CuO was much higher than that of Fe_2O_3 and more worthwhile to be used as the OC in the CLC system. However, disadvantages of CuO, such as high price, serious sintering, and possible environmental pollution, or Fe_2O_3 with its lower reactivity would obscure their usage in the realistic CLC system. Different from CuO and Fe_2O_3, the combined $CuFe_2O_4$ OC overcame some of the disadvantages of CuO and Fe_2O_3, and its mixture conversion index with LPS was greatly improved and reached 16.06%, far higher than $X_{LPS + Fe_2O_3}$ as 3.06%, and, thus, would be more advantageous to be used as the OC in the real CLC system.

Finally, with regard to the OC conversion alone in its mixture with coal, taken for the reaction of LPS with $CuFe_2O_4$ as an example, as shown in Figure 5a, the $CuFe_2O_4$ conversion index $X_{CuFe_2O_4\ (LPS)}$ in its reaction with LPS was 16.06%. This was bigger than that of 10.5% for the mixture conversion index of $CuFe_2O_4$ with LPS $X_{CuFe_2O_4 + LPS}$. Similar results could also be observed for all of the other reactions of LPS or YQ with those of the other two oxides, Fe_2O_3 or CuO, which clearly indicated that the real limiting step for the reaction of coal with different OCs is the coal pyrolysis and gasification, instead of its reaction with the OCs. Such a conclusion was in accordance with other findings.[2,4,8,10,11,15,23−25]

3.2.3. Multicycle of the Reduction/Oxidation Reaction of $CuFe_2O_4$ OC. To examine the reaction stability of $CuFe_2O_4$ over multiple cycles of the redox reactions, using the synthesized $CuFe_2O_4$ with SGCS as OC, four cycles of TGA experiments on the reduction of $CuFe_2O_4$ with H_2 and then oxidation with air at 850 °C were first conducted, as shown in Figure 6. Furthermore, because of the difficult TGA experiments for the redox reactions of $CuFe_2O_4$ with coal and air as mentioned above, only two cycles of redox reactions of $CuFe_2O_4$ with LPS or air in the same TGA setup were further carried out. The related experimental results are shown in Figure 7.

First, from Figure 6a, after each reduction of $CuFe_2O_4$ with 50 vol % H_2 for 8 min, the residual weight could be stabilized as around 75%, and then after oxidation with air for 5 min, the reduced counterpart of $CuFe_2O_4$ would be oxidized and reverted to its original state. Obviously, different from CuO,[7,26] $CuFe_2O_4$

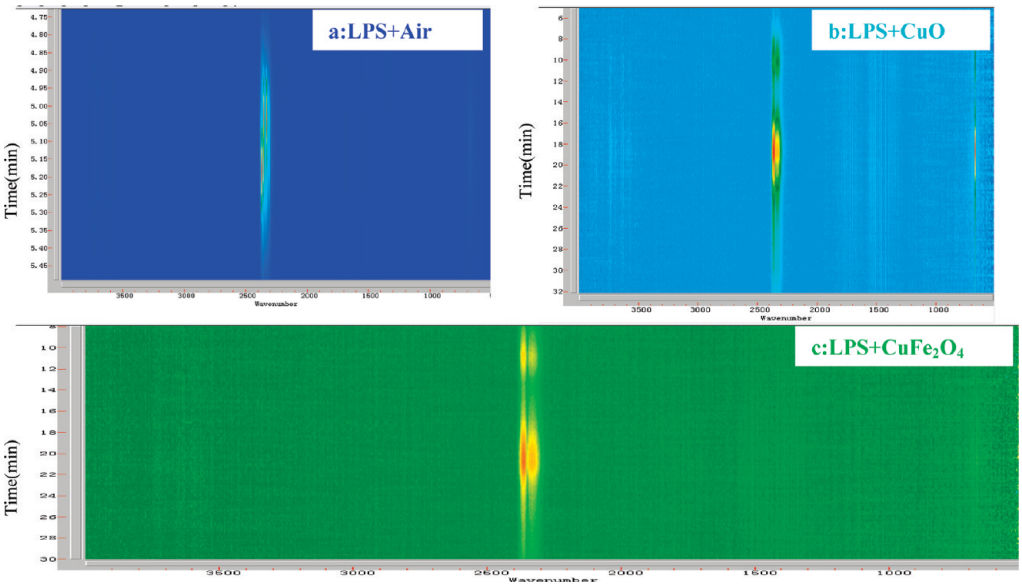

Figure 4. Two-dimensional IR plots for the reactions of LPS with different OCs: (a) LPS + air, (b) LPS + CuO, and (c) LPS + $CuFe_2O_4$.

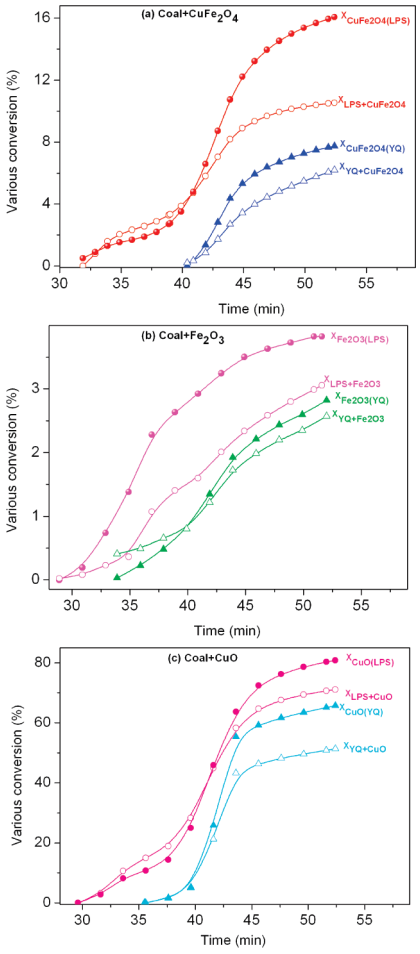

Figure 5. Conversions for the reactions of both coals (LPS and YQ) with different OCs: (a) coal + $CuFe_2O_4$, (b) coal + Fe_2O_3, and (c) coal + CuO.

synthesized with SGCS had enough reaction stability and good sintering resistance througout the whole redox reactions because

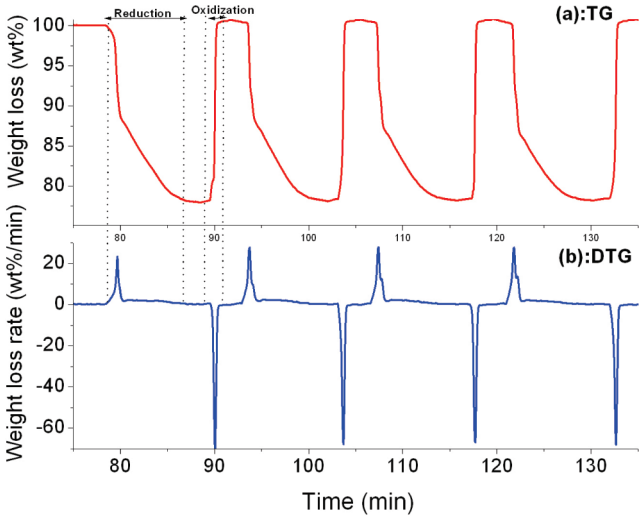

Figure 6. Four cycles of reduction of $CuFe_2O_4$ with H_2 (50 vol %) and then oxidation with air: (a) weight loss (TG) and (b) weight loss rate (DTG).

of great intensification of the sintering resistance of Cu by Fe present in the $CuFe_2O_4$ matrix.[27] Meanwhile, from Figure 6b, the maximal weight loss rate for each reduction of $CuFe_2O_4$ with H_2 was stabilized as ~26 wt %/min, less than half of the maximal oxidation weight loss rate around 67 wt %/min, which indicated that reduced $CuFe_2O_4$ could be easier to regenerate with air than its reduction with 50 vol % H_2. Thus, more attention should be paid to the reduction of $CuFe_2O_4$.

Furthermore, from Figure 7, for the two cycles of reduction of $CuFe_2O_4$ with LPS and then oxidation with air, the residual weight for the second reduction was a little increased to 90.76 wt % by 0.42 wt % relative to the final residual weights left after the first reduction, whereas the residual weight for the second oxidation was greatly decreased to 95.06 wt %, with the net decrease of 0.79 wt % . Acompanying the weight loss for the redox reaction of $CuFe_2O_4$ with LPS or air, from Figure 7b, the

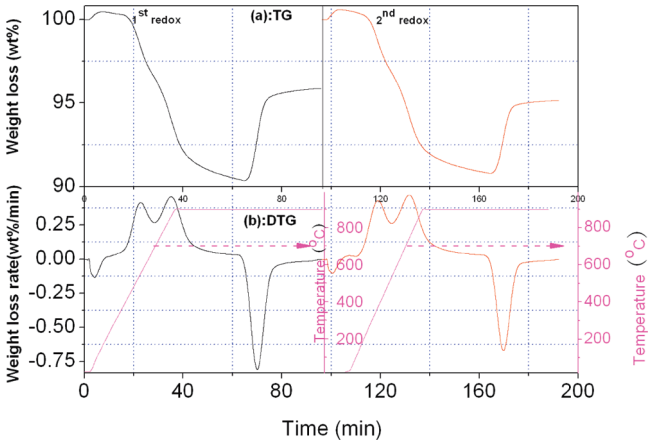

Figure 7. Two cycles of reduction and oxidation reactions between $CuFe_2O_4$ and LPS: (a) weight loss (TG) and (b) weight loss rate (DTG).

weight loss rates (DTG) of the reduction of $CuFe_2O_4$ with LPS for the two cycles were found to present a two-staged reaction and the DTG peaks were stabilized as 0.30 and 0.44 wt %/min, respectively. However, the maximum weight loss rates by oxidation of reduced $CuFe_2O_4$ with air were changed from −0.80 wt %/min at the first oxidation to −0.67%/min at the second oxidation, mainly because of the adverse effect from the coal ash left after each redox reaction of $CuFe_2O_4$ with LPS and air, as discussed in the following section.

3.2.4. Thermodynamic Simulation of the Reduction of $CuFe_2O_4$ with LPS. To gain a better understanding of both oxygen transfer for $CuFe_2O_4$, coal conversion, and minerals evolution during the redox reaction of $CuFe_2O_4$ with coal, LPS was selected as a model fuel in this research and a complex equilibrium system consisting of 376 species was designed, as shown in Table 3. The reaction of $CuFe_2O_4$ with LPS was simulated using equilibrium software HSC Chemistry, version 4.1, and the simulation results are presented in Figure 8.

In terms of LPS conversion during its reaction with $CuFe_2O_4$ from Figure 8a, CO_2 was observed to be dominant througout the whole reaction process of LPS with $CuFe_2O_4$ and its fraction increased from ∼87 to 93% at 400−800 °C; as followed, when the temperature was further increased to 1100 °C, there was a little drop of the CO_2 fraction from 93 to 92.2%. Meanwhile, the carbon matrix of LPS was quickly disintegrated with a sharp drop of the C content from 12.5% at 400 °C to nearly 0% at 800 °C, but the CO fraction was increased from 0% at 400 °C to 7.85% at 1100 °C, mainly because the lattice oxygen from $CuFe_2O_4$ transferable to LPS is not sufficient by the formation of inert compounds from the interaction of reduced $CuFe_2O_4$ with minerals in LPS. This fact will be discussed in more detail later. The predicted variations of CO_2 and CO concentrations with the temperature were in agreement with other experimental observations,[12,13] although the fuel and OC used differed.

In addition, from the inset of Figure 8a, it would be found out that less than 0.004% of CH_4 was generated from LPS pyrolysis below 700 °C and decreased with the increase of the temperature. However, different from CH_4, the fraction of COS ascended with the temperature above 750 °C, possibly because of some different reaction pathways involved,[28] such as $H_2S + CO \rightarrow H_2 + COS$, $H_2S + CO_2 \rightarrow H_2O + COS$, and $SO_2 + 3CO \rightarrow COS + 3CO_2$. Of course, sulfur species, such as H_2S and SO_2, were also

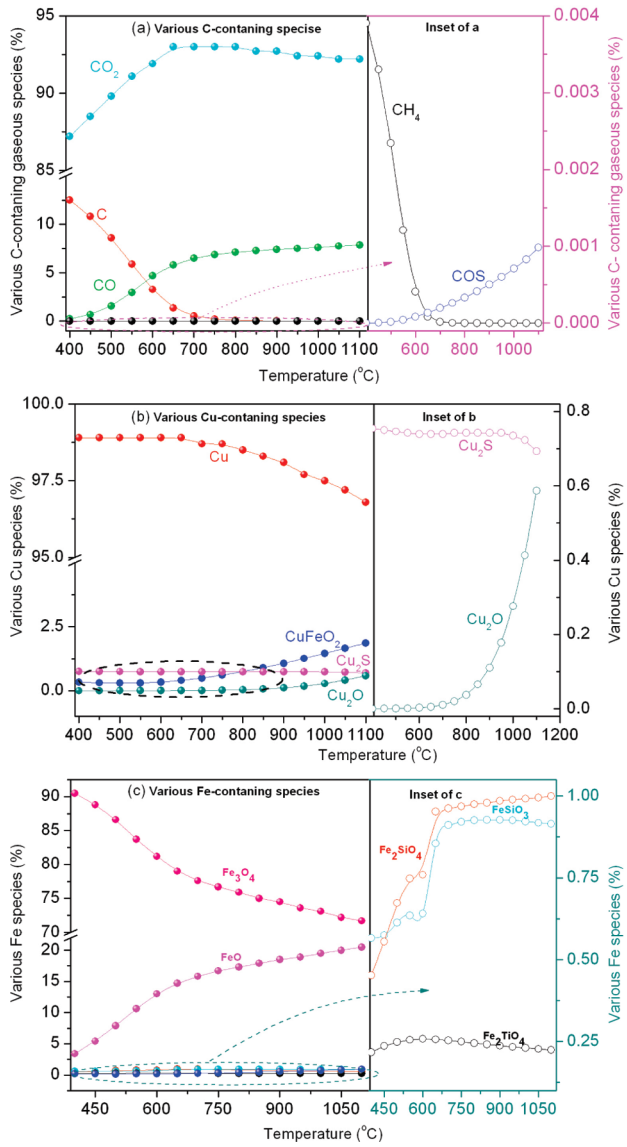

Figure 8. Equilibrium distribution of various species for the reduction of $CuFe_2O_4$ with LPS: (a) gaseous C-containing species, (b) Cu-containing species, and (c) various Fe-contaning species.

generated, but sulfur evolution for the reaction of LPS with $CuFe_2O_4$ is not the focus of this research and will be further investigated in the future.

In terms of $CuFe_2O_4$ evolution and oxygen transfer during its reaction with LPS, according to the distribution of Cu species in Figure 8b and Fe species in Figure 8c, the two dominant species evolved from $CuFe_2O_4$ were Cu and Fe_3O_4. The amounts of both Cu and Fe_3O_4 decreased throughout the whole temperature history (i.e., 400−1100 °C), which implied that, during the reaction of $CuFe_2O_4$ with LPS, $CuFe_2O_4$ was mainly reduced to Cu and Fe_3O_4 by transfer of the lattice oxygen [O] to LPS through the pathway below, similar to the reduction of $CuFe_2O_4$ with H_2,[29,30] CO,[31] or CH_4.[32]

$$CuFe_2O_4 \rightarrow Cu + Fe_3O_4 + [O] \quad (7)$$

Furthermore, from Figure 8c, the fraction of FeO was found to be always increasing from 3.41% at 400 °C to 20.5% at 1100 °C. On the basis of the fact of the increase in the CO fraction in Figure 8a,

the increased CO fraction promoted the further reduction of Fe_3O_4 to FeO by transferring more lattice oxygen [O] from Fe_3O_4 to LPS,[33] as shown in the expression below.

$$Fe_3O_4 \rightarrow FeO + [O] \quad (8)$$

Meanwhile, during the reaction of $CuFe_2O_4$ with LPS over 800 °C, as shown in Figure 8b, $CuFeO_2$ and Cu_2O were also found to occur and increase with the temperature, possibly because of the direct decomposition of $CuFe_2O_4$ into delafossite $CuFeO_2$, hematite, and oxygen, as shown in eq 9,[34−37] and then further partial decomposition of $CuFeO_2$ into cuprite Cu_2O and hematite Fe_2O_3, as shown in eq 10.[38,39]

$$4CuFe_2O_4 \rightarrow 4CuFeO_2 + 2Fe_2O_3 + O_2 \quad (9)$$

$$2CuFeO_2 \rightarrow Cu_2O + Fe_2O_3 \quad (10)$$

Especially, O_2 produced was greatly beneficial to the full conversion of the remaining coal, while the generated Fe_2O_3 was further reduced into Fe_3O_4 and other lower valence iron oxides than Fe_3O_4.[30,33] In addition, the greater percentages of Fe_3O_4 and Cu as compared to those of $CuFeO_2$ and FeO shown in panels b and c of Figure 8 clearly indicated that the dominant reaction pathway of $CuFe_2O_4$ with LPS was eq 7 coupled with eq 8 rather than eqs 9 and 10.

Finally, from the insets in panels b and c of Figure 8, it could be found that Cu in $CuFe_2O_4$ tended to react with various sulfur species emitted from LPS coal to form Cu_2S[40] but Fe in $CuFe_2O_4$ was preferred to react with minerals in LPS, especially SiO_2 under a reducing condition, to form both Fe_2SiO_4 and $FeSiO_3$.[12] It was considered that both the interactions of some reduced $CuFe_2O_4$ with minerals present in LPS and partial decompostion of $CuFe_2O_4$ into $CuFeO_2$ and Cu_2O meant that the amount of $CuFe_2O_4$ was not sufficient for the full oxidation of LPS. Overall, equilibrium simulation is helpful to better understand the mechanisms invovled for the reaction of LPS with $CuFe_2O_4$.

3.3. Chemical and Microstructural Analysis. To further clarify the reaction mechanisms involved and help understand the issue of ash separation from the reaction of coal with OC, the morphology and elemental composition of both residues from the reactions of LPS and YQ with $CuFe_2O_4$ were characterized using FSEM/EDX, as shown in Figure 9. Meanwhile, FSEM/EDX analyses of LPS and YQ pyrolysis residues under N_2 atmosphere are also provided in Figure 9 for references. The elemental compositions for the optionally selected spots on the FSEM image were calculated using the ZAF correction method and listed in Table 4. Furthermore, the detailed phases contained for the reaction of $CuFe_2O_4$ with these two Chinese coals were identified using XRD analysis, and the results are provided in Figure 10.

First, from Figure 9a, for the pyrolysis of LPS, the residues of LPS in the SEM pattern were observed to mainly consist of the relatively dark bulk material in spot 1 and the fragmentary discrete particles in spot 2. From the EDX analysis, the atomic fraction of C in spot 1 was 42.57%, higher than that in spot 2, possibly resulting from the main carbon matrix not completely disintegrated during LPS pyrolysis, while spot 2 was identified as minerals inherent in the carbon matrix, mainly composed of Si, Al, and O. Furthermore, as shown in Figure 10a, XRD analysis of the residue from LPS pyrolysis indicated that both SiO_2 and silicates, such as $CaAl_2Si_2O_8$, $CaFeSi_2O_6$, and $KFeSi_3O_8$, were the main mineral compositions. In addition, although most of the

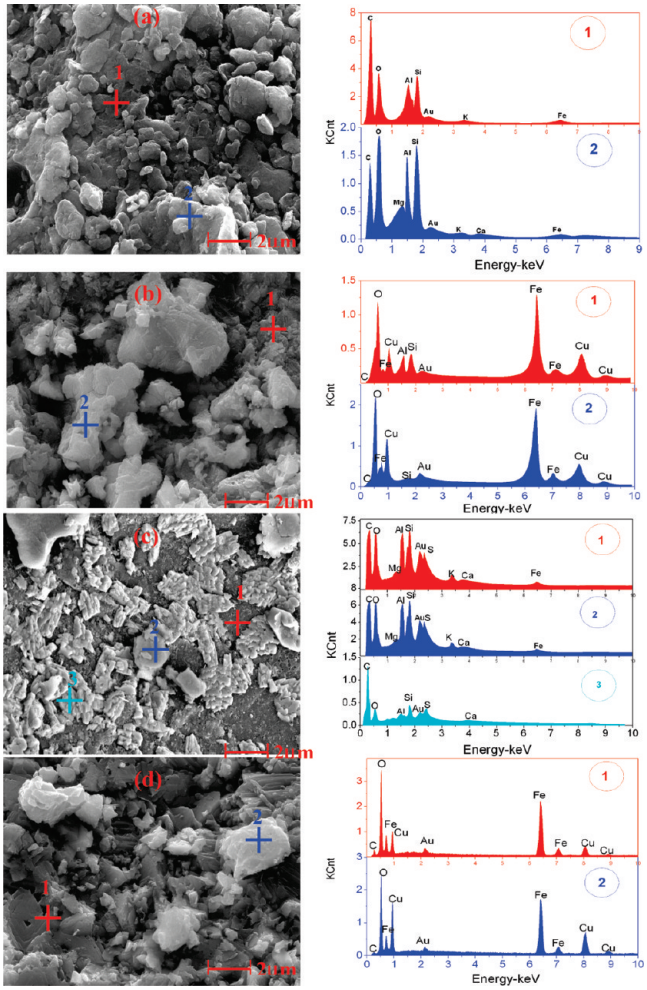

Figure 9. FSEM/EDX analysis of coals without and with $CuFe_2O_4$: (a) LPS pyrolysis under N_2 atmosphere, (b) reaction of LPS with $CuFe_2O_4$, (c) YQ pyrolysis under N_2 atmosphere, and (d) reaction of YQ with $CuFe_2O_4$.

residue should be ascribed to the carbon matrix by EDX analysis, it could not be detected in XRD analysis, mainly because of the amorphous characteristics of the derived carbon from LPS pyrolysis.[32,41]

Similar to LPS pyrolysis, as shown in Figure 9c, the SEM/EDX pattern of YQ pyrolysis revealed that the residues left were also made up of the main carbon matrix with C atomic fraction of 80.8% in spot 1 and some discrete minerals in either smooth particles in spot 2 or scaled bars by appearance in spot 3. These mineral particles were further identified by XRD analysis as SiO_2 and some different silicates from that of LPS, such as $Ca_3Fe_2(SiO_4)_3$ and $Mg_3Al_2Si_3O_{12}$.

Furthermore, from the SEM pattern in Figure 9b for the reaction of LPS with $CuFe_2O_4$ or Figure 9d for YQ with $CuFe_2O_4$, it could be observed that the residues were evenly distributed without discernible agglomeration or sintering and the atomic fractions of Cu, Fe, and O by EDX analysis in the optionally selected spots 1 or 2 were uniformly distributed around 16, 27, and 50%, respectively. Meanwhile, from Table 4, the atomic fraction of C for LPS with $CuFe_2O_4$ was below 1.6% and that for YQ with $CuFe_2O_4$ was less than 4%, far lower than those left after LPS and YQ pyrolysis, mainly because of the

Table 4. Elemental Analysis (Atomic %) of the Reaction of LPS and YQ with $CuFe_2O_4$ by FSEM/EDX, Applying the ZAF Correction Method

samples		C	O	Fe	Cu	Al	Si	S	K	Ca	Mg
LPS pyrolysis	spot 1	42.57	41.47	0.94	0	5.83	7.60	0.70	0.27	0.13	0.28
	spot 2	28.76	47.63	1.16	0	8.77	11.87	0.59	0.38	0.21	0.32
LPS + $CuFe_2O_4$	spot 1	1.00	42.89	26.72	16.73	5.94	5.83	0.25	0	0	0
	spot 2	1.57	53.63	28.59	14.37	0.40	0.52	0.08	0	0	0
YQ pyrolysis	spot 1	80.80	14.82	0.35	0	1.16	1.43	1.21	0	0.23	0
	spot 2	52.25	37.75	0.21	0	3.23	4.41	0.87	0.19	0.15	0.13
	spot 3	63.28	24.34	8.45	0	1.02	1.00	1.91	0	0	0
YQ + $CuFe_2O_4$	spot 1	3.74	58.61	27.59	8.74	0.35	0.26	0.17	0	0	0
	spot 2	1.62	52.96	25.78	18.25	0.52	0.33	0.12	0	0	0

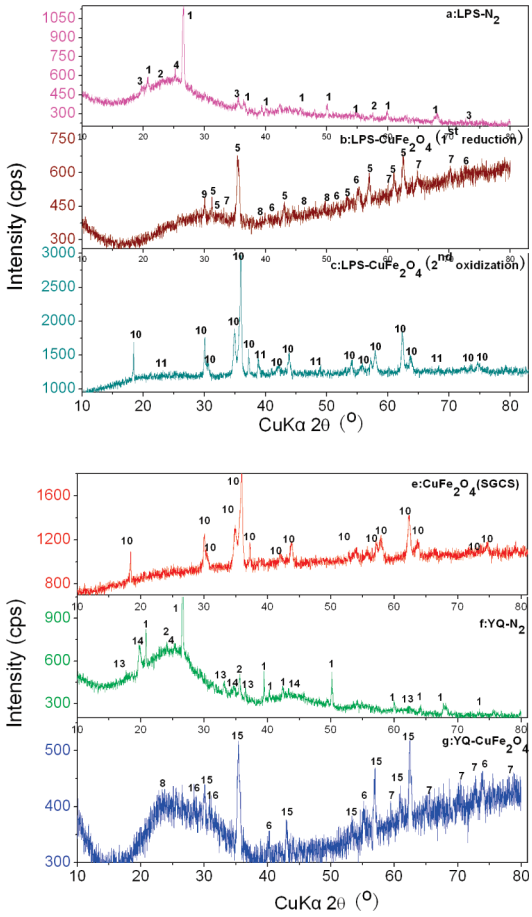

Figure 10. XRD study of the solid products of coals with $CuFe_2O_4$. In this figure, 1, quartz (SiO_2); 2, calcium aluminum silicate ($CaAl_2Si_2O_8$); 3, hedenbergite ($CaFeSi_2O_6$); 4, potassium iron silicate ($KFeSi_3O_8$); 5, magnetite ($Fe_{2.962}O_4$); 6, copper (Cu); 7, copper iron oxide ($CuFeO_2$); 8, fayalite (Fe_2SiO_4); 9, ferrosilite ($FeSiO_3$); 10, copper ferrite ($CuFe_2O_4$); 11, copper oxide (CuO); 12, iron ringwoodite (Fe_2SiO_4); 13, andradite [$Ca_3Fe_2(SiO_4)_3$]; 14, magnesium aluminum silicate ($Mg_3Al_2Si_3O_{12}$); 15, magnetite ($Fe_{2.957}O_4$); and 16, calcium aluminum silicate ($CaAl_2SiO_6$).

sufficient oxidation of C present in LPS or YQ by $CuFe_2O_4$. Of course, the catalytic function of reduced $CuFe_2O_4$ to gasification of the remaining carbon with steam should also be kept in mind.[31] Meanwhile, from XRD analysis of the reaction residues of $CuFe_2O_4$ with LPS or YQ in curves b and g of Figure 10, the reduced counterparts of $CuFe_2O_4$ with LPS were Cu, $CuFeO_2$, and $Fe_{2.962}O_4$ but the reduced counterparts of $CuFe_2O_4$ with YQ were Cu, $CuFeO_2$, and $Fe_{2.957}O_4$. According to the thermodynamic simulation in section 3.2.4, Cu was possibly derived from the reduction of $CuFe_2O_4$ throughout the whole reaction process at 400−1100 °C by eq 7, while $CuFeO_2$ was produced by the direct decomposition of $CuFe_2O_4$ at a temperature over 800 °C by eq 9, which was in accordance with the thermodynamic simulation above. However, oxygen-deficient iron oxides, such as $Fe_{2.962}O_4$ and $Fe_{2.957}O_4$, detected from XRD analysis were different from the predicted Fe species from thermodynamic simulation shown in Figure 8c. The disparity mainly resulted from the limited Fe species available in the HSC software library relative to those of XRD analysis. However, at least, the decrease of the Fe_3O_4 fraction together with the increase of the FeO fraction with the temperature from thermodynamic simulation in Figure 8c clearly revealed that the further reduction of Fe_3O_4 really occurred.

In addition, as shown in the curves b and g of Figure 10, Fe_2SiO_4 was also detected by XRD analysis in the samples of both LPS and YQ that had been reduced by $CuFe_2O_4$. Detected Fe_2SiO_4 mainly resulted from the interaction between FeO obtained from reduced $CuFe_2O_4$, as shown in eq 8, and SiO_2 contained in the LPS or YQ samples under the local reducing atmosphere.[12] Formed Fe_2SiO_4 not only lowered the melting point of the OC but also deteriorated the reactivity of the OC. Further research should be performed on this issue.

Finally, the reoxidation of reduced $CuFe_2O_4$ with air after its reduction with coal is also a great concern. According to XRD analysis, relative to fresh $CuFe_2O_4$ synthesized by SGCS in Figure 10d, reduced $CuFe_2O_4$ with the model coal LPS could be oxidized back to $CuFe_2O_4$ with a little CuO left. The reoxidized $CuFe_2O_4$ fraction could be estimated as 87.13% by the index $R_{CuFe_2O_4}$ below[25,28,42]

$$R_{CuFe_2O_4} = \frac{I_{CuFe_2O_4}}{I_{CuFe_2O_4} + I_{CuO}} \quad (11)$$

where $I_{CuFe_2O_4}$ and I_{CuO} are the majority XRD peaks of $CuFe_2O_4$ and CuO in Figure 10c, respectively. The reason for the presence of CuO was possibly that, during the reduction of $CuFe_2O_4$ with LPS, some reduced iron fractions in $CuFe_2O_4$ interacted with minerals (especially SiO_2) in LPS to form inactive compounds, such as Fe_2SiO_4, as discussed above, and resulted in insufficient Fe_2O_3 to combine with CuO and be reoxidized back into $CuFe_2O_4$. Therefore, great attention should be paid to the evolution of the minerals in CLC of coal, and measures should be taken to separate effectively the ash produced from reduced $CuFe_2O_4$.

4. CONCLUSION

$CuFe_2O_4$, as a novel OC, was put forward in this research. The reaction of $CuFe_2O_4$ with two Chinese coals of different ranks was performed in TGA and then systematically investigated using both thermodynamic simulation and different experimental means, including FTIR, FSEM/EDX, and XRD. Relevant conclusions were reached as follows: (1) TGA experiments for the reaction of LPS or YQ with $CuFe_2O_4$ were conducted. The results demonstrated that the reaction for LPS with $CuFe_2O_4$ underwent two distinct reaction stages at 300−600 and 600−850 °C but the reaction of YQ with $CuFe_2O_4$ displayed a single reaction stage above 600 °C. Meanwhile, for the reduction of $CuFe_2O_4$ with two Chinese coals, the maximum mass loss rates above 600 °C were more pronounced. (2) Two conversion indexes were established for the reduction of different OCs ($CuFe_2O_4$, Fe_2O_3, and CuO) with two Chinese coals, LPS and YQ. The OC conversion indices (i.e., $X_{OC\ (coal)}$) of three OCs in their mixtures with different coals were always bigger than their mixture conversion indices (i.e., $X_{coal\ +\ OC}$) for the three OCs with two Chinese coals, clearly indicating that the real limiting step for the reaction of coal with OCs is pyrolysis and gasification of coal instead of the reaction of coal with OCs. (3) Mechanisms involved for the reaction of $CuFe_2O_4$ with coal were explored using thermodynamic simulation. Reduction of $CuFe_2O_4$ into Cu and Fe_3O_4 (as shown in eq 7) was dominated by transfer of the lattice oxygen in $CuFe_2O_4$ to LPS throughout the whole reaction at 400−1100 °C. However, above 800 °C, direct decompostion of $CuFe_2O_4$ into $CuFeO_2$ by eq 9 and then further partial decomposition of $CuFeO_2$ into Cu_2O were commenced by eq 10. Meanwhile, Fe_2O_3 formed in eqs 9 and 10 would be further reduced. (4) Finally, FSEM/EDX and XRD analysis of the solid reduced residues of $CuFe_2O_4$ with LPS and YQ indicated that, besides Cu and $CuFeO_2$, oxygen-deficient iron oxides, such as $Fe_{2.962}O_4$ for LPS or $Fe_{2.957}O_4$ for YQ, were also generated.

■ AUTHOR INFORMATION

Corresponding Author

*Telephone: (27)87542417. Fax: (27)87542616. E-mail: david-wn@163.com.

■ ACKNOWLEDGMENT

This work is supported by the A*Star SERC Grant of Singapore (SERC 0921380025-M47070019), the National Natural Science Foundation of China (50906030 and 50936001), and partial funding from the National Basic Research Program (2010CB227003 and 2011CB707301). Special thanks should be presented to senior scientist Dr. Dongho Lee from Nanyang Technological University, editor Dr. Constance Senior, and other colleagues studying abroad for their careful revision of the manuscript. Meanwhile, the staff from the Analytical and Testing Center, Huazhong University of Science and Technology, were also appreciated for the related experimental analysis.

■ REFERENCES

(1) Jin, H.; Okamoto, T.; Ishida, M. Development of a novel chemical-looping combustion: Synthesis of a solid material NiO/$NiAl_2O_4$. *Ind. Eng. Chem. Res.* **1999**, *38* (1), 126–132.

(2) Berguerand, N.; Lyngfelt, A. Design and operation of a 10 kWth chemical-looping combustor for solid fuels—Testing with South African coal. *Fuel* **2008**, *87* (12), 2713–2726.

(3) Leion, H.; Mattisson, T.; Lyngfelt, A. Solid fuels in chemical-looping combustion. *Int. J. Greenhouse Gas Control* **2008**, *2* (2), 180–193.

(4) Shen, L. H.; Wu, J. H.; Gao, Z. P.; Xiao, J. Experiments on chemical looping combustion of coal with a NiO based oxygen carrier. *Combust. Flame* **2009**, *156* (3), 721–728.

(5) Cao, Y.; Pan, W.-P. Investigation of chemical looping combustion by solid fuels. 1. Process analysis. *Energy Fuels* **2006**, *20* (5), 1836–1844.

(6) Chandel, M. K.; Hoteit, A.; Delebarre, A. Experimental investigation of some metal oxides for chemical looping combustion in a fluidized bed reactor. *Fuel* **2009**, *88* (5), 898–908.

(7) Chuang, S. Y.; Dennis, J. S.; Hayhurst, A. N.; Scott, S. A. Development and performance of Cu-based oxygen carriers for chemical-looping combustion. *Combust. Flame* **2008**, *154* (1−2), 109–121.

(8) Siriwardane, R.; Tian, H. J.; Richards, G.; Simonyi, T.; Poston, J. Chemical-looping combustion of coal with metal oxide oxygen carriers. *Energy Fuels* **2009**, *23* (8), 3885–3892.

(9) Labiano-García, F.; Gayán, P.; Adánez, J.; De Díego, L.; Forero, C. R. Solid waste management of a chemical-looping combustion plant using Cu-based oxygen carriers. *Environ. Sci. Technol.* **2007**, *41*, 5882–5887.

(10) Cao, Y.; Casenas, B.; Pan, W.-P. Investigation of chemical looping combustion by solid fuels. 2. Redox reaction kinetics and product characterization with coal, biomass, and solid waste as solid fuels and CuO as an oxygen carrier. *Energy Fuels* **2006**, *20* (5), 1845–1854.

(11) Zhao, H. B.; Liu, L. M.; Wang, B. W.; Xu, D.; Jiang, L. L.; Zheng, C. G. Sol−gel-derived NiO/$NiAl_2O_4$ oxygen carriers for chemical-looping combustion by coal char. *Energy Fuels* **2008**, *22* (2), 898–905.

(12) Gu, H. M.; Shen, L. H.; Xiao, J.; Zhang, S. W.; Song, T. Chemical looping combustion of biomass/coal with natural iron ore as oxygen carrier in a continuous reactor. *Energy Fuels* **2011**, *25* (1), 446–455.

(13) Gu, H. M.; Wu, J. H.; Hao, J. G.; Shen, L. H.; Xiao, J. Experiments on chemical looping combustion of coal in interconnected fludized bed using hematite as oxygen carrier. *Proc. Chin. Soc. Electr. Eng.* **2010**, *30* (17), 51–56 (in Chinese).

(14) Wang, B. W.; Yan, R.; Lee, D. H.; Zheng, Y.; Zhao, H. B.; Zheng, C. G. Characterization and evaluation of Fe_2O_3/Al_2O_3 oxygen carrier prepared by sol−gel combustion synthesis. *J. Anal. Appl. Pyrolysis* **2011**, *91* (1), 105–113.

(15) Sun, X. Y.; Xiang, W. G.; Wang, S.; Tian, W. D.; Xu, X.; Xu, Y. J.; Xiao, Y. H. Investigation of coal fueled chemical looping combustion using Fe_3O_4 as oxygen carrier: Influence of variables. *J. Therm. Sci.* **2010**, *19* (3), 266–275.

(16) Mookherjee, S.; Ray, H. S.; Mukherjee, A. Thermogravimetric studies on the reduction of hematite ore fines by a surrounding layer of coal or char fines. Part 2. Non-isothermal kinetic studies. *Thermochim. Acta* **1985**, *95* (1), 247–256.

(17) Wang, B. W.; Yan, R.; Lee, D. H.; Liang, D. T.; Zheng, Y.; Zhao, H. B.; Zheng, C. G. Thermodynamic investigation of carbon deposition and sulfur evolution in chemical looping combustion with syngas. *Energy Fuels* **2008**, *22* (2), 1012–1020.

(18) Saha, C.; Roy, B.; Bhattacharya, S. Chemical looping combustion of Victorian brown coal using NiO oxygen carrier. *Int. J. Hydrogen Energy* **2011**, *36* (4), 3253–3259.

(19) Yang, H. P.; Chen, H. P.; Ju, F. D.; Yan, R.; Zhang, S. H. Influence of pressure on coal pyrolysis and char gasification. *Energy Fuels* **2007**, *21* (6), 3165–3170.

(20) Wang, J. Q.; Fang, M. X.; Luo, Z. Y.; Cen, K. F. Research on fast thermolysis kinetics of coal. *Proc. Chin. Soc. Electr. Eng.* **2007**, *27* (17), 18–22 (in Chinese).

(21) Leion, H.; Jerndal, E.; Steenari, B. M.; Hermansson, S.; Mattisson, T.; Lyngfelt, A. Solid fuels in chemical looping combustion using oxide scale and unprocessed iron ore oxygen carriers. *Fuel* **2009**, *88* (10), 1945–1954.

(22) Leion, H.; Lyngfelt, A.; Mattisson, T.; Lyngfelt, A. Solid fuels in chemical-looping combustion using a NiO-based oxygen carrier. *Chem. Eng. Res. Des.* **2009**, *87* (11), 1543–1550.

(23) Dennis, J. S.; Scott, S. A. In situ gasification of a lignite coal and CO_2 separation using chemical looping with a Cu-based oxygen carrier. *Fuel* **2010**, *89* (7), 1623–1640.

(24) Dennis, J. S.; Müller, C. R.; Scott, S. A. In situ gasification and CO_2 separation using chemical looping with a Cu-based oxygen carrier: Performance with bituminous coals. *Fuel* **2010**, *89* (9), 2353–2364.

(25) Shen, L. H.; Wu, J. H.; Gao, Z. P.; Xiao, J. Reactivity deterioration of NiO/Al_2O_3 oxygen carrier for chemical looping cmbustion of coal in 10 kW_{th} reactor. *Combust. Flame* **2009**, *156* (7), 1377–1385.

(26) de Díego, L. F.; Gayán, P.; García-Labiano, F.; Celaya, J.; Abad, A.; Adánez, J. Impregnated CuO/Al_2O_3 oxygen carriers for chemical-looping combustion: Avoiding fluidized bed agglomeration. *Energy Fuels* **2005**, *19* (5), 1850–1856.

(27) Faungnawakij, K.; Shimoda, N.; Fukunaga, T.; Kikuchi, R.; Eguchi, K. Cu-Based spinel catalysts CuB_2O_4 (B = Fe, Mn, Cr, Ga, Al, $Fe_{0.75}Mn_{0.25}$) for steam reforming of dimethyl ether. *Appl. Catal., A* **2008**, *341* (1−2), 139–145.

(28) Shen, L. H.; Gao, Z. P.; Wu, J. H.; Xiao, J. Sulfur behavior in chemical looping combustion with NiO/Al_2O_3 oxygen carrier. *Combust. Flame* **2010**, *157* (5), 853–863.

(29) Khedr, M. H.; Farghali, A. A. Microstructure, kinetics and mechanisms of CO_2 catalytic decomposition over freshly reduced nano-crystallite $CuFe_2O_4$ at 400−600 °C. *Appl. Catal., B* **2005**, *61* (3−4), 219–226.

(30) Shin, H.-C.; Choi, S.-C. Mechanism of M ferrites (M = Cu and Ni) in the CO_2 decomposition reaction. *Mater. Chem.* **2001**, *13* (4), 1238–1242.

(31) Estrella, M.; Barrio, L.; Zhou, G.; Wang, X. Q.; Wang, Q.; Wen, W.; Hanson, J. C.; Frenkel, A. I.; Rodriguez, J. A. In situ characterization of $CuFe_2O_4$ and Cu/Fe_3O_4 water−gas shift catalysts. *J. Phys. Chem. C* **2009**, *113* (32), 14411–14417.

(32) Kang, K.-S.; Kim, C.-H.; Cho, W.-C.; Bae, K.-K.; Woo, S.-W.; Park, C.-S. Reduction characteristics of $CuFe_2O_4$ and Fe_3O_4 by methane; $CuFe_2O_4$ as an oxidant. *Int. J. Hydrogen Energy* **2008**, *33* (17), 4560–4568.

(33) Jozwiak, W. K.; Kaczmarerk, E.; Maniecki, T. P.; Ignaczak, W.; Maniukiewicz, W. Reduction behavior of iron oxides in hydrogen and carbon monoxide atmospheres. *Appl. Catal., A* **2007**, *326* (1), 17–27.

(34) Kenfack, F.; Langbein, H. Influence of the temperature and the oxygen partial pressure on the phase formation in the system Cu−Fe−O. *Cryst. Res. Technol.* **2004**, *39* (12), 1070–1079.

(35) Katkov, A. E.; Lykasov, A. A. Spinel phase relation in the Fe_3O_4−$CuFe_2O_4$ system. *Inorg. Mater.* **2003**, *39* (2), 171–174.

(36) Jacob, K. T.; Alcock, C. B.; Fitzner, K. Activities in the spinel solid solution, phase equilibria and thermodynamic properties of thernary phases in the system Cu−Fe−O. *Metall. Trans. B* **1977**, *8B* (3), 451–460.

(37) Zhang, P.; Yu, B.; Zhang, L. Mechanism of oxygen releasing of copper ferrite in the formation of the corresponding oxygen-deficient compound. *Sci. China, Ser. B: Chem.* **2009**, *52* (1), 101–108.

(38) Zhao, T. R.; Takei, H. Study of the oxidizaton and reduction kinetics of copper iron oxide[$CuFeO_2$] in the Cu−Fe−O system. *Mater. Res. Bull.* **1977**, *32* (10), 1377–1393.

(39) Kaneko, H.; Tokoyama, T.; Fuse, A.; Ishihara, H.; Hasegawa, N.; Tamaura, Y. Synthesis of new ferrite, Al−Cu ferrite, and its oxygen deficiency for solar H_2 generation from H_2O. *Int. J. Hydrogen Energy* **2006**, *31* (15), 2256–2265.

(40) Solunke, R. D.; Veser, G. Integrating desulfurization with CO_2-capture in chemical-looping combustion. *Fuel* **2011**, *90* (2), 608–617.

(41) Kang, K.-S.; Kim, C.-H.; Bae, K.-K.; Cho, W.-C.; Kim, W.-J.; Kim, Y.-H.; Kim, S.-H.; Park, C.-S. Redox cycling of $CuFe_2O_4$ supported on ZrO_2 and CeO_2 for two-step methane reforming/water splitting. *Int. J. Hydrogen Energy* **2010**, *35* (2), 568–576.

(42) Selvan, R. K.; Augustin, C. O.; Berchmans, L. J.; Saraswathi, R. Combustion synthesis of $CuFe_2O_4$. *Mater. Res. Bull.* **2003**, *38* (1), 41–54.